JOURNAL OF AGRICULTURAL AND FOOD CHEMISTRY

pubs.acs.org/JAFC Article

Competitive Lateral Flow Immunoassay Relying on Au−SiO_2 Janus Nanoparticles with an Asymmetric Structure and Function for Furazolidone Residue Monitoring

Lihong Su, Lulu Wang, Jingke Xu, Zonghan Wang, Xiaolin Yao, Jing Sun, Jianlong Wang, and Daohong Zhang*

Cite This: *J. Agric. Food Chem.* 2021, 69, 511−519 Read Online

ACCESS | Metrics & More | Article Recommendations | Supporting Information

ABSTRACT: Gold nanoparticles (AuNPs) are the most commonly used signal materials in lateral flow immunoassay (LFIA). However, the assay sensitivity of traditional AuNP-based LFIA is usually limited by the incomplete competition between free target analytes and immobilized antigens for the binding of AuNP-labeled antibodies. To unfreeze this limitation, here, asymmetric Au−SiO_2 Janus NPs (about 66 nm) were designed and synthesized. Au−SiO_2 Janus NPs can assemble into snowman-like anisotropic structures and combine two different physicochemical properties at their opposite sides, where the AuNP side mainly possesses the antibody conjugating and signal providing functions and the SiO_2 side primarily offers the stable function. In virtue of the unique asymmetric nanostructure, only the AuNP side can interact with target analytes by specific antigen−antibody interactions, which could significantly improve the efficiency of competition. Selecting furazolidone as a model analyte, the immunoassay biosensor showed a limit of detection as low as 0.08 ng/mL, 10-fold decreased than that of the AuNPs-LFIA. Moreover, the Au−SiO_2 Janus NP lateral flow immunoassay was well applied in chicken, pork, honey, and beef food samples with visual detection limits of 0.8 ng/g, 0.16 ng/g, 0.4 ng/mL, and 0.16 ng/g, respectively. The Au−SiO_2 Janus NPs possess the advantages of both materials, which will broaden their applications as a potential alternative in the rapid and sensitive detection of antibiotic residues.

KEYWORDS: *Au−SiO_2 Janus nanoparticle, asymmetric structure, lateral flow immunoassay, furazolidone*

INTRODUCTION

Furazolidone (FZD), an important antibacterial agent, is widely used to treat a variety of bacterial or pathogenic microbial infections in agriculture.[1] Although FZD is effective in preventing disease and promoting the growth of food-producing animals, long-term intake of food products containing FZD residue could result in numerous side effects, such as potential carcinogenic, mutagenesis, and teratogenic effects.[2,3] FZD can be rapidly metabolized in the body, whereas its metabolite 3-amino-2-oxazolidinone (AOZ) remains highly stable.[4] In most cases, the AOZ derivative of 3-[(2-nitrophenyl) methylene-amino]-2-oxazolidinone (CPAOZ) is actually detected by LFIAs for monitoring the FZD residue in food.

Lateral flow immunoassay (LFIA) has been widely applied in food safety monitoring due to its desirable features of simple equipment, easy operation, and rapid target capturing.[5,6] In general, the detection of antibiotic residues is mainly based on competitive immunoassay. AuNP is a commonly used signal label in the field of LFIA analysis, owing to its simple operation, easy labeling, and unique optical properties.[7] Unfortunately, conventional AuNP-based LFIAs often suffer from drawbacks of low stability and sensitivity, which have significantly hindered their further applications in complex food environmental and ultratrace target detection.[8−10] Various new nanoparticles have been reported to improve the analytical performance of LFIA, including metal oxide, chemiluminescent, and florescent materials[11−13] However, the problem of inefficient binding still remains in the competitive LFIAs.[14] Consequently, some methods have been developed to overcome this limitation, such as adjustment of the threshold level, bridge-, and orientation antibody.[15−17] However, when many antibody molecules are simultaneously labeled on a nanoparticle, the binding of free targets with a probe cannot inhibit the interaction between the coated antigen and the same probe, leading to ineffective competition and low sensitivity, especially for targets of low concentration. Although the effectiveness of the competition can be enhanced by reducing the labeling amount of the antibody, it also gives rise to a weak detection signal, which is not conducive to the LFIA construction.

A Janus nanoparticle, as a signal label with a unique asymmetric structure and functional asymmetry, may provide a new insight for the above problems and has been used in drug delivery, optical imaging, and morphological template.[18−21] Compared with the homogeneous nanostructure, Janus nanoparticles can be composed of two distinct parts with

Received: September 18, 2020
Revised: December 14, 2020
Accepted: December 17, 2020
Published: December 29, 2020

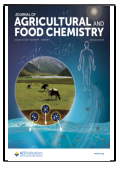

https://dx.doi.org/10.1021/acs.jafc.0c06016
J. Agric. Food Chem. 2021, 69, 511−519

different physicochemical properties in one nanostructure, facilitating the creation of signal tags with different functions. Particularly, among the most exciting materials, a silica nanoparticle (SiO_2 NP) has been widely applied due to its excellent biocompatibility and chemical stability in biosensing.[22−24] The introduction of a silica layer on AuNP has been proved to be effective in protecting and preventing AuNP from aggregation, owing to a high negative charge.[25−27] Interestingly, asymmetric Au−SiO_2 Janus NP not only holds different functionalities on opposite sides but maintains a favorable localized surface plasmon resonance property as well.[28] In the preparation of a Au−SiO_2 Janus NP-based probe, the antibody is just selectively oriented on a part of the exposed surface of AuNPs with a significantly decreased labeling amount, which can provide more opportunities to adjust the contradiction between the detection signals and competition efficiency.

Herein, through a wet chemical strategy, asymmetric Au−SiO_2 Janus NP was synthesized and used as a signal tag in the LFIA for rapid and sensitive detection of CPAOZ. The silica layer can be asymmetrically deposited on AuNP in virtue of segregation of two different ligands on the AuNP surface. Importantly, the Au side of Au−SiO_2 Janus NP was used to couple with an antibody, which could effectively reduce the labeling consumption of the antibody and refrain from affecting by incomplete competition. Moreover, compared with pure AuNP, the asymmetric Au−SiO_2 Janus NP with bifunctional anisotropic properties can effectively prevent the aggregation of AuNPs and thus increase the colloidal stability. To demonstrate its feasibility and practicability, multiple food samples were detected for the CPAOZ residue using the Au−SiO_2 Janus NP-based LFIA. This work put forward a sample, rapid, and sensitive method for small-molecule detection in food safety, laying a foundation for Janus nanomaterial application in other related areas.

EXPERIMENTAL SECTION

Materials and Apparatus. Hydrogen tetrachloroaurate (III) hydrate ($HAuCl_4·3H_2O$), trisodium citrate, 2-propanol, ammonia (NH_3, 25%), and tetraethyl orthosilane (TEOS) were obtained from Aladdin Chemistry Co., Ltd. (Shanghai, China). Bovine serum albumin (BSA) and poly-(acrylic acid) (PAA) (M_W: 5000) were bought from Macklin Biochemical Co., Ltd. (Shanghai, China). 4-Mercaptophenylacetic acid (4-MPAA, 97%) was purchased from Alfa Aesar (Beijing, China). A monoclonal antibody (mAb) against CPAOZ (1E9) was produced in our laboratory. A nitrocellulose (NC) membrane, glass fiber, poly(vinyl chloride) plate, and absorbent pad were purchased from Kingdiag-Biotech Co., Ltd. (Shanghai, China). Chicken, honey, pork, and beef were purchased from a local market (Xianyang, China).

The transmission electron microscopy (TEM) images were taken on a JEM-1230 electron microscopy (Tokyo, Japan). The X-ray diffraction (XRD) patterns were acquired on Bruker D8 Advanced X-ray Diffractometer (Karlsruhe, Germany). Ultraviolet−visible (UV−vis) spectra were acquired in the 400−800 nm range with a spectrophotometer (UV-2550) (Shimadzu, Japan). The X-ray photoelectron spectroscopy (XPS) was recorded using an Axis Ultra DLD X-ray photoelectron spectrometer. The ζ potential measurements were obtained using a Zetasizer Nano-ZS dynamic light scattering instrument (Malvern, U.K.). The nanoparticle tracking analysis (NTA) was performed on a ZetaView PMX 110 (Particle Metrix, Germany).

Synthesis of the AuNPs. AuNPs were prepared by the citrate reduction process.[29] Briefly, 1 mL of a 1% (w/v) $HAuCl_4·3H_2O$ solution was mixed with 98 mL of water and heated under vigorous stirring. When the mixed solution started to boil, 1 mL of 1% (w/v) trisodium citrate was rapidly added to the solution. After the color changed from yellow to fuchsia, the mixture was continually stirred for 10 min and finally stored at 4 °C.

Synthesis of the Au−SiO_2 Janus NPs. Au−SiO_2 Janus NPs were synthesized according to the previous literature with some modifications.[30] First, after the centrifugation of 8 mL of a AuNP solution at 12 000 rpm, the collected AuNPs were dispersed in 500 μL of deionized water and added into 2.5 mL of 2-propanol under vigorous stirring. Then, 20 μL of 4-MPAA (5 mM in ethanol) and 60 μL of PAA (0.65 mM) were added into the above mixture under continuous stirring for 30 min, followed by pouring into 600 μL of TEOS (8.9 mM) and 90 μL of ammonia. After 12 h of the reaction, Au−SiO_2 Janus NPs were obtained by washing three times with water. Finally, Au−SiO_2 Janus NPs were dispersed in 8 mL of water and stored at 4 °C before use.

Preparation of the Au−SiO_2 Janus NPs and AuNP-Based Probes. Initially, 4 μg of anti-CPAOZ mAb (1 mg/mL) was added to 1 mL of a Au−SiO_2 Janus NP deionized water solution and reacted for 2 h at room temperature. Following this, 100 μL of BSA (10%) was added to block unconjugated active sites on the surface of Au−SiO_2 Janus NPs for another 30 min. At last, the prepared Au−SiO_2 Janus NP probes were washed three times with water by centrifugation at 12 000 rpm and then dissolved in 100 μL of 2 mM borax buffer (pH 9.0) containing 0.02% sodium azide and 0.1% PEG-200 000 (w/v).

Anti-CPAOZ mAb was labeled with AuNPs also based on a physical interaction. Briefly, 8 μg of mAb was added into 1 mL of a AuNP solution at pH 8.0−9.0 under gentle shaking for 30 min, followed by addition of 100 μL of BSA (10%) for another 2 h to block the free binding sites at 4 °C. Then, the AuNP probes were obtained by centrifugation at 12 000 rpm for 10 min and washed twice by 2 mM borax buffer. Finally, the resulted AuNP probes were suspended in 100 μL of borate buffer and stored at 4 °C.

Preparation of the Lateral Flow Immunoassay Strip. The lateral flow immunoassay strip was made of a sample pad, conjugate pad, nitrocellulose membrane, and absorbent pad. First, the sample pad and conjugate pad were pretreated by soaking in a blocking buffer solution and dried at 37 °C for 12 h. CPAOZ-BSA and goat antimouse IgG were dispensed on the NC as a test (T) line and control (C) line, respectively. After drying, all different parts were laminated onto a plastic adhesive backing pad with 1 mm overlap. Finally, they were cut into 3 mm wide strips and stored in a dry condition before use.

Detection Performance of the Au−SiO_2 Janus NPs-LFIA. For evaluating the sensitivity, different concentrations of CPAOZ standards were spiked in a solution containing 100 μL of phosphate-buffered saline (PBS) and 4 μL of a Au−SiO_2 Janus NP probe (or 4 μL of AuNP probe), and then the mixture was added onto the sample pad. After 8 min of the reaction, the result of detection was observed by naked eyes as colorimetric evaluation, and the image of the test line was processed by imageJ software to obtain the corresponding gray value.

Detection of CPAOZ in Food Samples. The chicken, pork, honey, and beef samples were confirmed to be CPAOZ free in advance by the high-performance liquid chromatography. Then, 1 g of the ground meat sample (for chicken, pork, and beef) or 0.5 mL of honey was suspended and well mixed in 5 mL of PBS buffer by the previous research with some modifications.[13,31] The honey sample suspension was spiked by the CPAOZ standard to obtain a final concentration of 0.04, 0.08, 0.4, 0.8, 1, and 2 ng/mL. The meat samples at 0.08, 0.16, 0.8, 1.6, 2, and 4 ng/g were prepared by adding an appropriate volume of the CPAOZ standard. After sonication for 15 min, the sample supernatant was collected by centrifugation and evaluated by the proposed LFIA under optimal conditions. At the end of 8 min of the migration reaction, the strip was observed by naked eyes as a semiquantitative readout.

RESULTS AND DISCUSSION

Discussion on Advantages of the Au−SiO_2 Janus NPs-LFIA. In this work, an asymmetric Au−SiO_2 Janus NP

https://dx.doi.org/10.1021/acs.jafc.0c06016
J. Agric. Food Chem. 2021, 69, 511−519

Scheme 1. Advantage Illustration of the Au−SiO_2 Janus NPs and Au−SiO_2 Janus NP-Based LFIA[a]

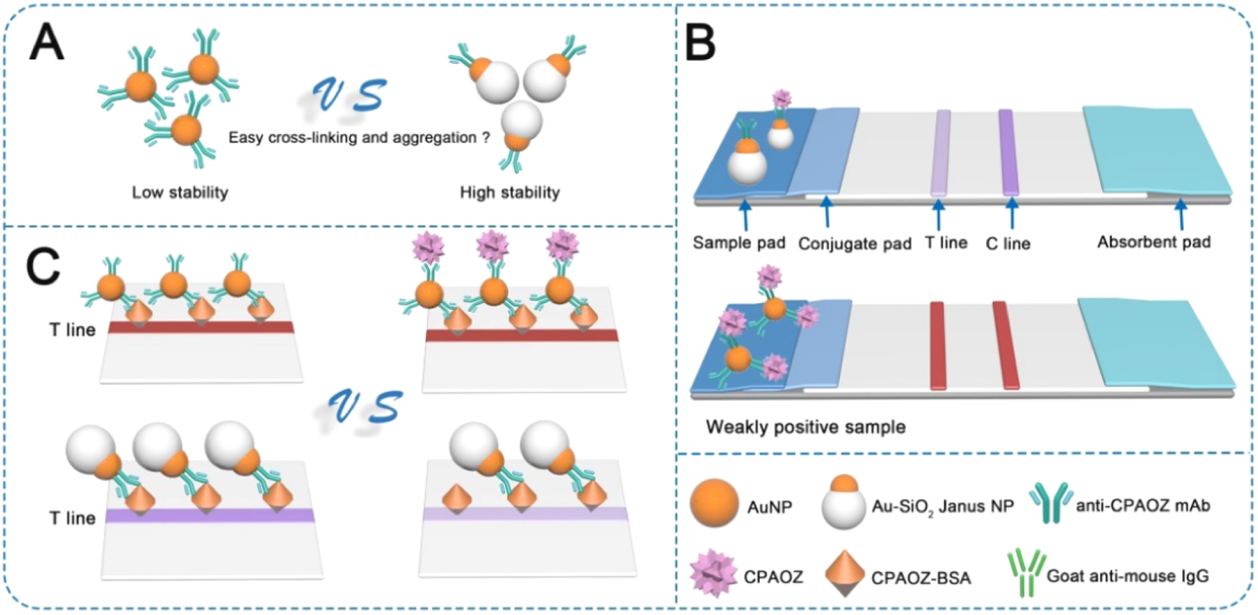

[a](A) Comparison between the Au−SiO_2 Janus NPs and AuNPs, (B) comparison of response sensitivity for weakly positive samples by the Au−SiO_2 Janus NPs and AuNP-based LFIAs, and the (C) enlarged illustration of the T line for the competition efficiency of the target analyte in the Au−SiO_2 Janus NPs and AuNP-based LFIAs.

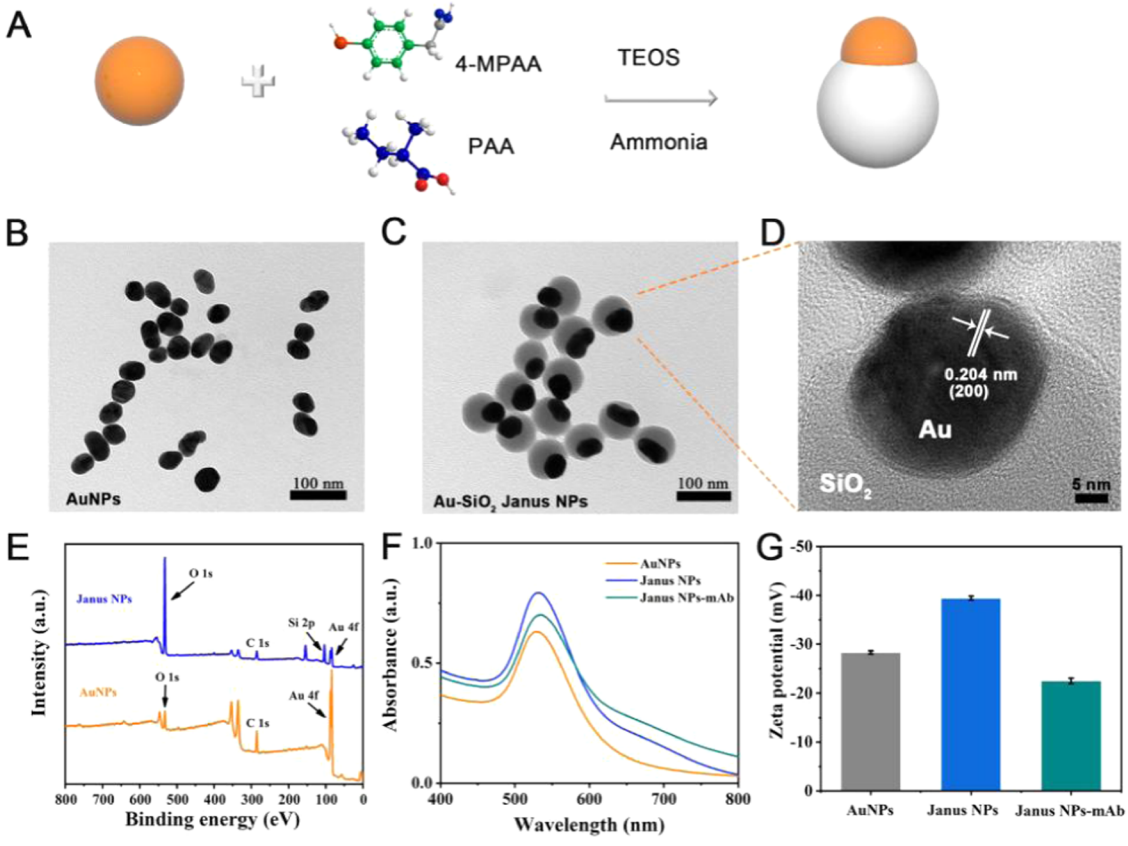

Figure 1. (A) Synthesis schematic of the Au−SiO_2 Janus NP, (B) TEM image of AuNPs, (C) TEM image of Au−SiO_2 Janus NPs, (D) HTEM image of Au−SiO_2 Janus NPs, (E) XPS wide spectra of AuNPs and Au−SiO_2 Janus NPs, (F) UV−vis spectra of AuNPs, Au−SiO_2 Janus NPs, and Au−SiO_2 Janus NPs-mAb, and (G) ζ potentials of AuNPs, Au−SiO_2 Janus NPs, and Au−SiO_2 Janus NPs-mAb.

was used as a new signal substrate to realize the sensitive colorimetric detection of CPAOZ by the lateral flow immunoassay (Scheme 1). First, the silica layer partially coated on the AuNPs could efficiently improve the stability of the probe by effectively avoiding the cross-linking and aggregation of probes, while the exposed gold surfaces were

https://dx.doi.org/10.1021/acs.jafc.0c06016
J. Agric. Food Chem. 2021, 69, 511−519

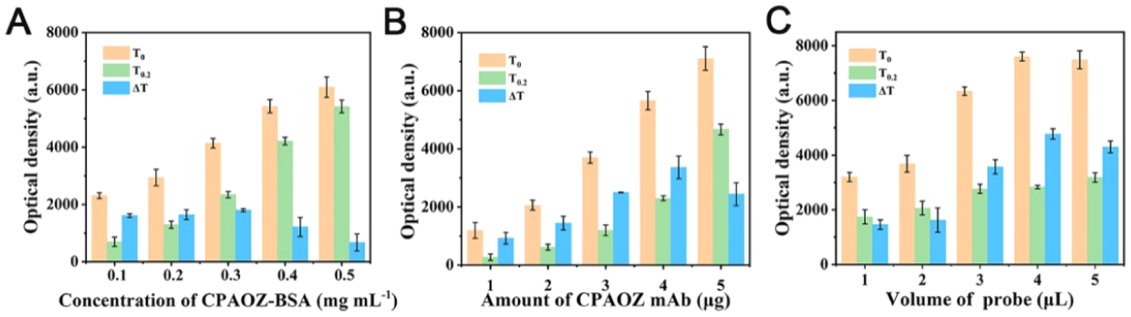

Figure 2. Optimization results of parameters for the Au−SiO_2 Janus NPs-LFIA. (A) Concentration of CPAOZ-BSA, (B) amount of anti-CPAOZ mAb, and the (C) volume of Au−SiO_2 Janus NPs-mAb probe. Error bar: standard error (n = 3).

responsible for the optical performance (Scheme 1A). Additionally, in the preparation of the probe, antibody molecules can be selectively oriented to the AuNP region. The competitive sensitivity of free AuNP-based LFIAs is likely to be influenced by the incomplete competition between free small molecules and immobilized complete antigens for the binding of AuNP-labeled antibodies (Scheme 1B). For example, there is a possibility that a AuNPs-mAb probe, which has been retained on the NC membrane through combining with the immobilized complete antigen, will also bind the free target analytes if more than one antibody molecule is fixed on the surface of the same nanoparticle in the probe, resulting in inaccurate response between the concentration of free target analytes and signal intensity. While, for the asymmetric Au−SiO_2 Janus NP, due to the steric hindrance effect of SiO_2 and because part of the particle was covered by SiO_2, for each AuNP, only very limited antibody could be bound on the surface of AuNP compared to that on the free AuNP, which could evidently improve the competition efficiency of target analytes in the competitive LFIA by avoiding the "ineffective combination" between the AuNP-based probe and target small molecules. It is inescapably clear that in comparison with free AuNP, Au−SiO_2 Janus NP-based LFIA could produce more sensitive signal response under a low level of free CPAOZ (Scheme 1C).

Synthesis and Characterization of Au−SiO_2 Janus NPs. Au−SiO_2 Janus NPs were synthesized through a simple wet chemical method. 4-MPAA and PAA were employed as competitive ligands to regulate the silica layer selectively deposited on the surface of AuNP, achieving the nanostructure of Au−SiO_2 Janus NP (Figure 1A). As shown in Figure 1B, the initial AuNPs have a spherical morphology with an average size of around 35 nm. Au−SiO_2 Janus nanoparticles were optimized by adjusting the volume of aqueous ammonia. As shown in Figure S1A, when 30 μL of aqueous ammonia was added, aggregation occurs for the AuNPs due to incomplete hydrolysis of TEOS.[32] When 180 μL of aqueous ammonia was added, more than one AuNP is enclosed into the silicon sphere (Figure S1C) and cannot form the snowman-like Janus structure. While, as shown in Figure S1B, when 90 μL of aqueous ammonia was added, Au−SiO_2 Janus nanoparticles could be well synthesized as the desired snowman-like Janus structure with a size of about 66 nm (Figure 1C). Moreover, the size of AuNP is still 35 nm, demonstrating that AuNP has no aggregation during the synthesis process.[33] Correspondingly, the high-resolution TEM (HTEM) image of Au−SiO_2 Janus NPs (Figure 1D) reveals a clear lattice fringe with an interlayer spacing of 0.204 nm, which could be attributed to the (200) plane of a Au crystal.[34] In addition, X-ray photoelectron spectroscopy (XPS) was used to further elucidate the surface elemental compositions. As displayed in Figure 1E, the fully scanned spectra confirmed the existence of Au, C, and O elements in the AuNP sample, and Au, C, O, and Si elements in the Au−SiO_2 Janus NP sample, which are in good agreement with the desired components.[35] The high-resolution spectrum of Au 4f is fitted by two peaks at 84.0 and 87.7 eV, which could be assigned to $4f_{7/2}$ and $4f_{5/2}$ for metallic Au^0 species (Figure S2).[36] Furthermore, the UV−vis spectra of AuNPs exhibit an absorption peak at 528 nm in Figure 1F. As the SiO_2 shell formed, Au−SiO_2 Janus NPs exhibit a 5 nm red shift because the coating of silica on Au increased the local refractive index.[35] As compared with the ζ potential of AuNPs, the large negative charge of Au−SiO_2 Janus NPs further demonstrate the successful silica nanoshell modification on AuNP (Figure 1G).[37] The results indicate the successful synthesis of Au−SiO_2 Janus NPs.

To prove the successful formation of a signal probe, UV−vis absorption and ζ potential of Janus NPs-mAb were also carried out. As shown in Figure 1F, the absorption peak red-shifted to 536.5 nm resulted from the conjugation of anti-CPAOZ mAb with Au−SiO_2 Janus NPs. Additionally, the ζ potential of the probe was −22.5 mV (Figure 1G), indicating a positive shift of the Au−SiO_2 Janus NPs.[38] All of these proof prove that Au−SiO_2 Janus NPs successfully conjugate with an antibody.

To verify that antibody molecules were selectively oriented to the AuNP region in the Au−SiO_2 Janus NP, a comparison test of antibody coupling amounts on different nanomaterial of SiO_2, AuNPs, and Au−SiO_2 Janus NPs was carried out. Excess anti-CPAOZ mAb was added to the Janus, AuNPs, and SiO_2 suspensions. Unconjugated anti-CPAOZ mAb was quantified using a NanoDrop assay, and the amount of the fixed antibody was calculated as the difference between the total antibody added and the excess antibody remaining in the supernatant. As displayed in Figure S3, the highest coupling amount of the antibody appeared on AuNPs compared with Janus and SiO_2. The decrease of the antibody coupling amount on Janus is caused by the presence of silica, which on the one hand cannot effectively bind antibody molecules onto its surface, and on the other hand, can block the absorption of some antibody molecules onto the surface of AuNPs. Moreover, we calculated the number of antibodies for Au−SiO_2 Janus NPs and AuNPs by the nanoparticle tracking analysis (NTA) and NanoDrop assay. By calculation (Table S3), ∼6620 and ∼3460 antibody molecules are loaded per AuNP and Janus, respectively. These results further demonstrate that antibody molecules can be selectively oriented to the AuNP region.

Parameter Optimization of the Au−SiO_2 Janus NPs-LFIA. To obtain the best analytical performance, some

https://dx.doi.org/10.1021/acs.jafc.0c06016
J. Agric. Food Chem. 2021, 69, 511−519

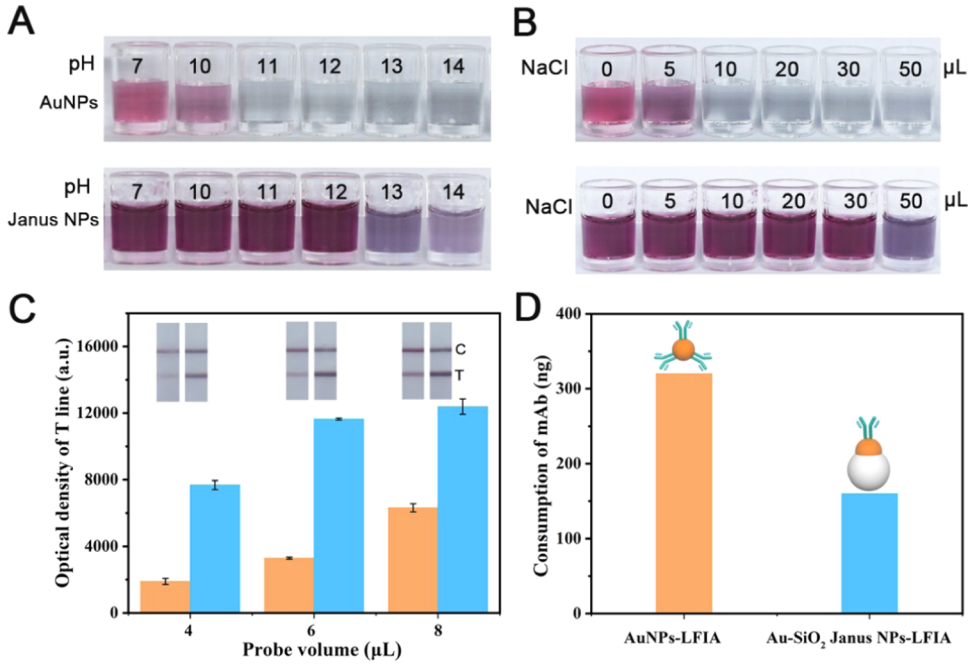

Figure 3. Colloid stabilities of AuNPs and Au−SiO_2 Janus NPs exposed at different pH values (A) and volumes of 10% NaCl (B). Optical densities of the T line corresponding to different volumes of the conventional AuNPs-LFIA (yellow) probe and the Au−SiO_2 Janus-LFIA (blue) probe, respectively. The inset shows relevant images of strip test results. (C) Antibody consumption per test of AuNPs-LFIA and Au−SiO_2 Janus-LFIA (D). Error bar: standard error (n = 3).

experimental parameters such as the concentration of CPAOZ-BSA, the amount of anti-CPAOZ mAb, and the volume of the Au−SiO_2 Janus NP probe were all optimized in detail. In the competitive immunoassay, an excellent competitive inhibition effect will generate a higher sensitivity. To get a satisfied competition effect, the competitive inhibition rate ΔT ($\Delta T = T_0 - T_{0.2}$, T_0 represents the T line optical density of a negative sample, and $T_{0.2}$ represents the T line optical density of the CPAOZ standard solution at 0.2 ng/mL) was selected as an indicative index.[39] As a competitor, CPAOZ-BSA can directly affect the detection sensitivity of LFIA. As shown in Figure 2A, ΔT reached a maximal value when the concentration of CPAOZ-BSA increased to 0.3 from 0.1 mg/mL, and then gradually decreased with the further increase of the CPAOZ-BSA concentration. To achieve a higher sensitivity and proper optical density, 0.3 mg/mL was chosen as the optimal parameter of CPAOZ-BSA.

In the preparation of a nanoparticle-labeled antibody probe, a minimum coupling amount of the antibody was needed to stabilize the nanomaterials from aggregation.[40] As shown in Figure S5, the absorbance of Au−SiO_2 Janus NPs obviously decreases at 1−2 μg, thus 3 μg of an antibody is considered as the minimum stable amount of the antibody required to stabilize the Janus NPs. However, in the competitive LFIA, the signal probe not only needs to label fewer antibodies to ensure the best competitive effect but also needs to ensure that the color signals can achieve the requirement of visual detection. As shown in Figure 2B, ΔT gradually rose with the labeling amount of mAb increasing from 1 to 4 μg and then dropped when the amount further increased to 5 μg. Therefore, 4 μg of anti-CPAOZ mAb was selected to modify Au−SiO_2 Janus NPs. Meanwhile, the volume of Au−SiO_2 Janus NP probes indirectly influences the detection sensitivity, especially for competitive immunoreactions. As displayed in Figure 2C, ΔT continuously elevated in the probe volume range of 1−4 μL and began to decline after 4 μL. Thus, 4 μL was considered as the optimal probe volume. Other extraessential but important experimental parameters for the Au−SiO_2 Janus NP-based LFIA biosensor are listed in Table S1, Figure S6.

Promotion Validation of Au−SiO_2 Janus NPs. Colloidal stability is an important factor for the LFIA detection, especially in the analysis of food with complex matrices. AuNPs and Au−SiO_2 Janus NP solutions with various pH values and addition volumes of NaCl were evaluated to unveil their colloidal stabilities. As shown in Figure 3A, compared with AuNPs, Au−SiO_2 Janus NPs have a better tolerance to pH. The colloidal Au−SiO_2 Janus NPs were stable until pH 13, while Au−SiO_2 Janus NPs started to aggregate, which may be caused by the dissolution of SiO_2, leading to the cross-linking of bare AuNPs.[41] A salt ion as another stability factor was evaluated and is shown in Figure 3B. NaCl (0−50 μL, 10%) and Au−SiO_2 Janus NPs or AuNPs (final volume: 0.5 mL) were mixed to analyze the stability. With the salt ion volume increased to 10 μL, the color of AuNPs changed from red to colorless, resulting from the aggregation of AuNPs. Whereas, the color of Au−SiO_2 Janus NPs did not show any obvious change until the NaCl volume reached 50 μL. These results reveal that Au−SiO_2 Janus NPs are more stable than AuNPs when exposed to high pH and salt ion levels. The excellent stability should be owing to the unique structure of Au−SiO_2 Janus NPs with a high negative charge, which has the capability of preventing the cross-linking and aggregation between nanoparticles. So, we can conclude that SiO_2 can serve as a protector for the significant improvement of colloidal stability.

To illuminate the signal enhancement function of Au−SiO_2 Janus NPs, AuNPs and Au−SiO_2 Janus NPs probes were compared in the LFIA with different volumes. In this section, 4 μg of anti-CPAOZ mAb was separately labeled on AuNPs and Au−SiO_2 Janus NPs to prepare probes. As shown in Figure 3C, when 4 μL of the probe is added, the color intensity of the T

https://dx.doi.org/10.1021/acs.jafc.0c06016
J. Agric. Food Chem. 2021, 69, 511−519

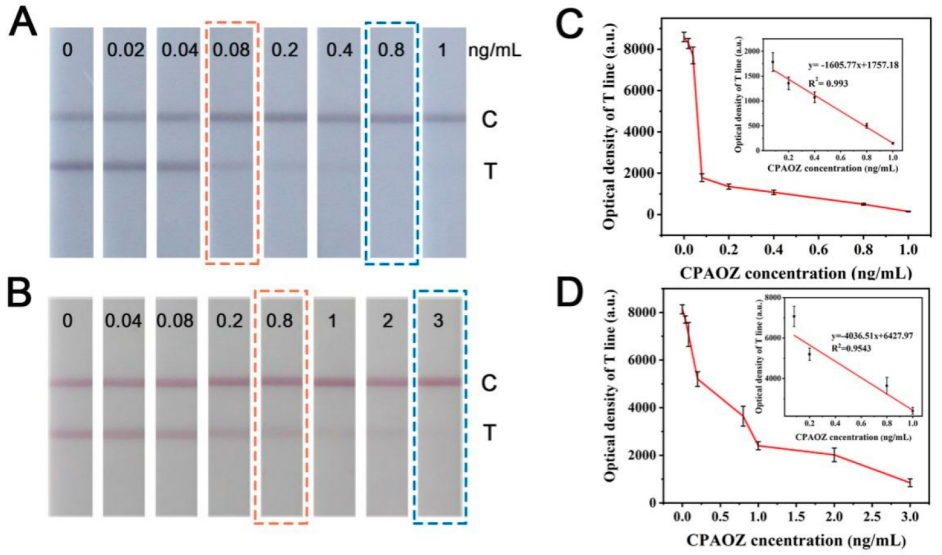

Figure 4. (A) Detection results of the CPAOZ standard solution by the Au−SiO_2 Janus NPs-LFIA. (B) Detection results of the CPAOZ standard solution by the AuNPs-LFIA. (C) Relationship between the CPAOZ concentration and optical density of the T line in PBS (inset image: the calibration curve of CPAOZ) based on the Au−SiO_2 Janus NPs-LFIA. (D) Relationship between the CPAOZ concentration and optical density of the T line in PBS (inset image: the calibration curve of CPAOZ) based on the AuNPs-LFIA. Error bar: standard error (n = 3). The brown dotted lines show the visual detection limits and blue dotted lines show the cutoff values.

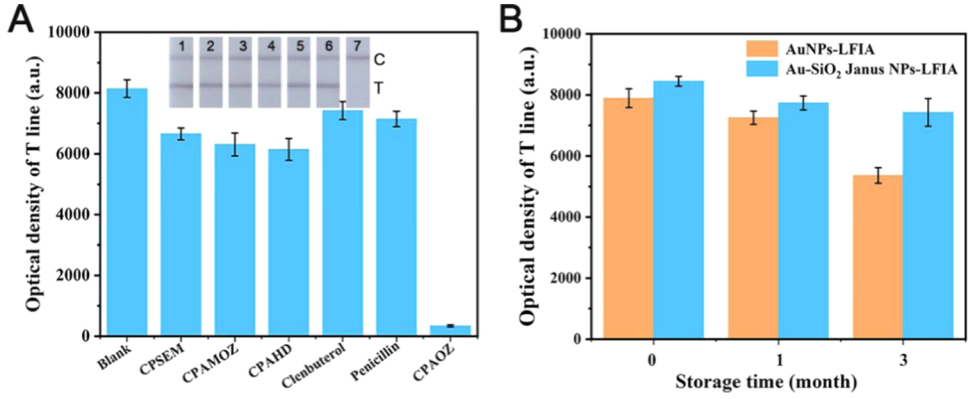

Figure 5. (A) Specificity performance of the Au−SiO_2 Janus NPs-LFIA. The concentration of CPAOZ was 1 ng/mL, concentrations for other interferences were all 100 ng/mL. The inset shows the relevant images of strip test results. (B) Stabilities of the Au−SiO_2 Janus NPs-LFIA and AuNPs-LFIA under 4 °C for 3 months. Error bar: standard error (n = 3).

line is very weak on the conventional strip, but the T line of the Au−SiO_2 Janus NP-based strip can be clearly observed. The T line of the conventional strip cannot be clearly seen until the AuNPs-mAb probe reached 8 μL, where the color intensity of AuNPs-mAb is still lower than that of the Janus NPs-mAb in 4 μL. In addition, the AuNPs-LFIA requires a much bigger antibody consumption than that of the Au−SiO_2 Janus NPs-LFIA per LFIA both under the optimal conditions (Figure 3D). The above results well validate the promotion function of the Au−SiO_2 Janus NPs in both the better stability and signal enhancement, which would contribute to the assay performance of Au−SiO_2 Janus NP-based LFIA.

Analytical Performance. On the basis of this immunoassay biosensor, we conducted a series of detection with CPAOZ standard solutions. The detection limit is defined as the minimum analyte level that can generate a clear and weaker color development in the T line of the test strip than that of the negative control strip. As CPAOZ concentration increased, fewer and fewer probes were anchored onto the T line and the purple color intensity became very weak under competitive-type detection. As displayed in Figure 4A, when the CPAOZ concentration increased to 0.08 ng/mL, the color intensity of the T line was obviously weaker than that on the negative strip. The color of the T line completely disappeared at 0.8 ng/mL due to the complete suppression to the competitive response. Therefore, 0.08 ng/mL CPAOZ is considered to be the visual detection limit for this immunoassay biosensor. Figure 4C shows the corresponding grayscale values; the optical density of the T line decreased with the increase of the CPAOZ concentration and exhibited a good linear R^2 = 0.993 in the range of 0.08−1 ng/mL. For comparison, a conventional AuNP-based immunoassay biosensor was also investigated. As shown in Figure 4D, AuNPs-LFIA exhibits a linear R^2 = 0.954 in the range of 0.08−1 ng/mL. As can be seen in Figure 4B, the visual detection limit is 0.8 ng/mL, which is 10-fold higher than that of the Au−SiO_2 Janus NP-based LFIA. In addition, compared with other methods, the LFIA based on Au−SiO_2 have a lower cutoff value and less antibody consumption (Table S4).

https://dx.doi.org/10.1021/acs.jafc.0c06016
J. Agric. Food Chem. 2021, 69, 511−519

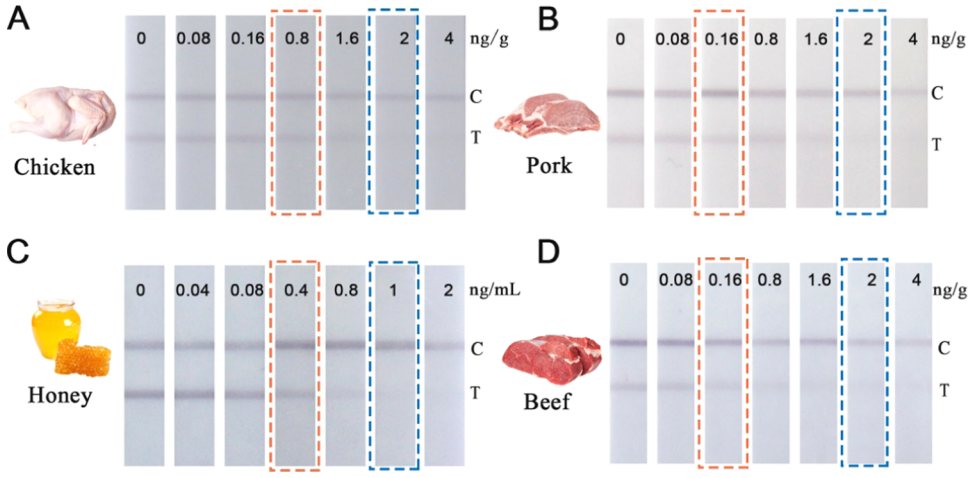

Figure 6. Detection results of CPAOZ in (A) chicken, (B) pork, (C) honey, and (D) beef samples based on the Au−SiO_2 Janus NPs-LFIA.

To evaluate the specificity of the immunoassay biosensor toward CPAOZ, several interferences including 4-[[2-(amino-carbonyl) hydrazinylidene] methyl]-benzoic acid (CPSEM), 4-[5-(morpholino-methyl)-2-oxooxazolidin-3-ylimino]methyl benzoic acid (CPAMOZ), 1-[(4-carbo-benzylidene)-amino]-imidazolidin-2,4-dione (CPAHD), clenbuterol, and penicillin, were investigated. The optical density separately corresponding to 1 ng/mL CPAOZ and as high as 100 ng/mL of interferences was compared based on the Au−SiO_2 Janus NPs-LFIA. As shown in Figure 5A, the visible color intensity of the T line toward each interference is almost the same as that of the blank strip, while no visible color of the T line can be seen on the strip corresponding to CPAOZ. There is also no big gap between the T line densities of strips for interferences and the blank strip. The results suggest that the immunoassay biosensor has a high anti-interference capability for CPAOZ identification. Meanwhile, the precision and reproducibility were tested by determining intra-assay and interassay coefficients of variation (CV). The reproducibility of the immunoassay biosensor was observed via using honey sample spiked by 0.08 and 0.4 ng/mL CPAOZ. As revealed in Table S2, both CVs of intra-assay and interassay are all below 6%, displaying the persuasive repeatability performance of this method. To preliminarily determine the storage stability, the immunosensor was stored at 4 °C for 3 months. As shown in Figure 5B, after storage for 3 months, the T line optical density of Au−SiO_2 Janus NPs-LFIA showed no obvious change, but that corresponding to AuNPs-LFIA apparently decreased. Therefore, the Au−SiO_2 Janus NP-LFIA has a better stability than AuNP-based LFIA after long-term storage.

Applicability Validation of the Au−SiO_2 Janus NPs-LFIA in Food Samples. Based on excellent analytical performances, the Au−SiO_2 Janus NPs-LFIA was applied for CPAOZ detection in food samples, including chicken, pork, honey, and beef. CPAOZ standards at different concentrations in food samples were measured by the Au−SiO_2 Janus NP-LFIA biosensor. As illustrated in Figure 6, colors of the T line completely disappear when the content level of CPAOZ reaches 2 ng/g in three meat samples and 1 ng/mL in the honey sample. The visual detection limits are 0.4 ng/mL, 0.8 ng/g, 0.16 ng/g, and 0.16 ng/g for the proposed method toward CPAOZ detection in honey, chicken, pork, and beef samples, respectively. To evaluate the reliability of the sampling technique, chicken and honey samples were also detected by conventional AuNPs-LFIA. As shown in Figure S7, AuNPs-LFIA is well applied in food samples. Moreover, Au−SiO_2 Janus NP-based LFIA shows a high sensitivity compared with the AuNP-based method in chicken and honey samples. Besides, the regulatory demand about the maximum residue limit (MRL) for furazolidone and its metabolites in Commission Decision 2003/181/EC is 1.0 ng/g.[42] Compared with the MRL demands, sensitivities of the proposed method in food samples are acceptable. From the results, we could assert that food samples did not or interfered little with the detection of CPAOZ, and the performances of the Au−SiO_2 Janus NP-LFIA biosensor were slightly influenced by matrices of the four samples, presenting a great application potential for AOZ residue monitoring in food samples.

In summary, by introducing asymmetric Au−SiO_2 Janus NPs, we fabricated a novel LFIA biosensor for CPAOZ detection. Owing to the unique structure, Au−SiO_2 Janus NPs showed excellent performances, such as the asymmetric coupling capability toward an antibody, the outstanding colloid stability under high pH, and salt ion level, which were beneficial for reducing antibody consumption and increasing competitive efficiency in the LFIA. The detection limit of Au−SiO_2 Janus NPs-LFIA was as low as 0.08 ng/mL, which showed a 10-fold enhancement in sensitivity compared to that of the AuNPs-LFIA. Moreover, the Au−SiO_2 Janus NPs-LFIA showed excellent selectivity toward the target analyte and acceptable reproducibility. In addition, the proposed immunoassay biosensor had expected applicability in food samples for the detection of CPAOZ. We believe that the as-synthesized anisotropic Janus nanoparticle could be used as an ideal candidate signal substrate, and this work will offer a reference for the application of other antibiotic residues in food.

■ ASSOCIATED CONTENT

Supporting Information

The Supporting Information is available free of charge at https://pubs.acs.org/doi/10.1021/acs.jafc.0c06016.

TEM images of Janus; the XPS survey spectrum; the evaluation of the mAb coupling amount; the UV spectra change of AuNPs and Au−SiO_2 Janus NPs with different amounts of the antibody after adding 10% NaCl; parameter optimization for the AuNP-LFIA; detection time of Au−SiO_2 NP LFIA; detection results of CPAOZ

https://dx.doi.org/10.1021/acs.jafc.0c06016
J. Agric. Food Chem. 2021, 69, 511−519

in (A) chicken and (B) honey based on the AuNP-LFIA; optimal parameters for the Au−SiO_2 Janus NP-based LFIA biosensor; the number of antibodies per particle for AuNP and Au−SiO_2 Janus NP-based probes; reproducibility analysis of the proposed LFIA for CPAOZ in honey samples; and the comparative evaluation of the LFIAs for FZD detection (PDF)

AUTHOR INFORMATION

Corresponding Author

Daohong Zhang − *College of Food Science and Engineering, Northwest A&F University, Xianyang 712100, Shaanxi, China;* orcid.org/0000-0003-2989-9761; Phone: +86 29-8709-2275; Email: zhangdh@nwsuaf.edu.cn

Authors

Lihong Su − *College of Food Science and Engineering, Northwest A&F University, Xianyang 712100, Shaanxi, China*

Lulu Wang − *College of Food Science and Engineering, Northwest A&F University, Xianyang 712100, Shaanxi, China*

Jingke Xu − *College of Food Science and Engineering, Northwest A&F University, Xianyang 712100, Shaanxi, China*

Zonghan Wang − *College of Food Science and Engineering, Northwest A&F University, Xianyang 712100, Shaanxi, China*

Xiaolin Yao − *College of Food Science and Engineering, Northwest A&F University, Xianyang 712100, Shaanxi, China*

Jing Sun − *Qinghai Key Laboratory of Qinghai-Tibet Plateau Biological Resources, Northwest Institute of Plateau Biology, Chinese Academy of Sciences, Xining 810008, Qinghai, China*

Jianlong Wang − *College of Food Science and Engineering, Northwest A&F University, Xianyang 712100, Shaanxi, China;* orcid.org/0000-0002-2879-9489

Complete contact information is available at: https://pubs.acs.org/10.1021/acs.jafc.0c06016

Notes

The authors declare no competing financial interest.

ACKNOWLEDGMENTS

The authors thank the National Natural Science Foundation of China (31972150, 21675127), the key R & D Projects in Shaanxi Province (2019NY-109), the Key Industries Innovation Chain Project of Shaanxi Province (2019ZDLSF07−08), the 417 Development Project of Qinghai Provincial Key Laboratory (2017-ZJ-Y10), and the Shaanxi Provincial Science Fund for Distinguished Young Scholars (2018JC-011).

REFERENCES

(1) Kokulnathan, T.; Wang, T.-J. Vanadium Carbide-Entrapped Graphitic Carbon Nitride Nanocomposites: Synthesis and Electrochemical Platforms for Accurate Detection of Furazolidone. *ACS Appl. Nano Mater.* **2020**, *3*, 2554−2561.

(2) Hwa, K.-Y.; Sharma, T. S. K.; Karuppaiah, P. Development of an electrochemical sensor based on a functionalized carbon black/tungsten carbide hybrid composite for the detection of furazolidone. *New J. Chem.* **2019**, *43*, 12078−12086.

(3) Chen, S.; Chen, X.; Zhang, L.; Gao, J.; Ma, Q. Electrochemiluminescence Detection of Escherichia coli O157:H7 Based on a Novel Polydopamine Surface Imprinted Polymer Biosensor. *ACS Appl. Mater. Interfaces* **2017**, *9*, 5430−5436.

(4) Lu, X.; Liang, X.; Dong, J.; Fang, Z.; Zeng, L. Lateral flow biosensor for multiplex detection of nitrofuran metabolites based on functionalized magnetic beads. *Anal. Bioanal. Chem.* **2016**, *408*, 6703−6709.

(5) Nguyen, V. T.; Song, S.; Park, S.; Joo, C. Recent advances in high-sensitivity detection methods for paper-based lateral-flow assay. *Biosens. Bioelectron.* **2020**, *152*, No. 112015.

(6) Quesada-González, D.; Merkoçi, A. Nanoparticle-based lateral flow biosensors. *Biosens. Bioelectron.* **2015**, *73*, 47−63.

(7) Li, J.; Duan, H.; Xu, P.; Huang, X.; Xiong, Y. Effect of different-sized spherical gold nanoparticles grown layer by layer on the sensitivity of an immunochromatographic assay. *RSC Adv.* **2016**, *6*, 26178−26185.

(8) Jiang, T.; Song, Y.; Wei, T.; Li, H.; Du, D.; Zhu, M. J.; Lin, Y. Sensitive detection of Escherichia coli O157:H7 using Pt-Au bimetal nanoparticles with peroxidase-like amplification. *Biosens. Bioelectron.* **2016**, *77*, 687−694.

(9) Phan, L. M. T.; Rafique, R.; Baek, S. H.; Nguyen, T. P.; Park, K. Y.; Kim, E. B.; Kim, J. G.; Park, J. P.; Kailasa, S. K.; Kim, H. J.; Chung, C.; Shim, T. S.; Park, T. J. Gold-copper nanoshell dot-blot immunoassay for naked-eye sensitive detection of tuberculosis specific CFP-10 antigen. *Biosens. Bioelectron.* **2018**, *121*, 111−117.

(10) Xing, Y.; Zhou, Y.; Zhang, Y.; Zhang, C.; Deng, X.; Dong, C.; Shuang, S. Facile Fabrication Route of Janus Gold-Mesoporous Silica Nanocarriers with Dual-Drug Delivery for Tumor Therapy. *ACS Biomater. Sci. Eng.* **2020**, *6*, 1573−1581.

(11) Hu, J.; Zhang, Z. L.; Wen, C. Y.; Tang, M.; Wu, L. L.; Liu, C.; Zhu, L.; Pang, D. W. Sensitive and Quantitative Detection of C-Reaction Protein Based on Immunofluorescent Nanospheres Coupled with Lateral Flow Test Strip. *Anal. Chem.* **2016**, *88*, 6577−6584.

(12) Ouyang, H.; Wang, W.; Shu, Q.; Fu, Z. Novel chemiluminescent immunochromatographic assay using a dual-readout signal probe for multiplexed detection of pesticide residues. *Analyst* **2018**, *143*, 2883−2888.

(13) Yao, X.; Wang, Z.; Dou, L.; Zhao, B.; He, Y.; Wang, J.; Sun, J.; Li, T.; Zhang, D. An innovative immunochromatography assay for highly sensitive detection of 17β-estradiol based on an indirect probe strategy. *Sens. Actuators, B* **2019**, *289*, 48−55.

(14) Urusov, A. E.; Petrakova, A. V.; Zherdev, A. V.; Dzantiev, B. B. "Multistage in one touch" design with a universal labelling conjugate for high-sensitive lateral flow immunoassays. *Biosens. Bioelectron.* **2016**, *86*, 575−579.

(15) Di Nardo, F.; Cavalera, S.; Baggiani, C.; Giovannoli, C.; Anfossi, L. Direct vs Mediated Coupling of Antibodies to Gold Nanoparticles: The Case of Salivary Cortisol Detection by Lateral Flow Immunoassay. *ACS Appl. Mater. Interfaces* **2019**, *11*, 32758−32768.

(16) Zvereva, E. A.; Byzova, N. A.; Sveshnikov, P. G.; Zherdev, A. V.; Dzantiev, B. B. Cut-off on demand: adjustment of the threshold level of an immunochromatographic assay for chloramphenicol. *Anal. Methods* **2015**, *7*, 6378−6384.

(17) Li, G.; Xu, L.; Wu, W.; Wang, D.; Jiang, J.; Chen, X.; Zhang, W.; Poapolathep, S.; Poapolathep, A.; Zhang, Z.; Zhang, Q.; Li, P. On-Site Ultrasensitive Detection Paper for Multiclass Chemical Contaminants via Universal Bridge-Antibody Labeling: Mycotoxin and Illegal Additives in Milk as an Example. *Anal. Chem.* **2019**, *91*, 1968−1973.

(18) Qin, W.; Peng, T.; Gao, Y.; Wang, F.; Hu, X.; Wang, K.; Shi, J.; Li, D.; Ren, J.; Fan, C. Catalysis-Driven Self-Thermophoresis of Janus Plasmonic Nanomotors. *Angew. Chem. Int. Ed.* **2017**, *56*, 515−518.

(19) Wu, Z.; Li, L.; Liao, T.; Chen, X.; Jiang, W.; Luo, W.; Yang, J.; Sun, Z. Janus nanoarchitectures: From structural design to catalytic applications. *Nano Today* **2018**, *22*, 62−82.

(20) Yánez-Sedeño, P.; Campuzano, S.; Pingarrón, J. M. Janus particles for (bio)sensing. *Appl. Mater. Today* **2017**, *9*, 276−288.

(21) Yang, H.-C.; Xie, Y.; Hou, J.; Cheetham, A. K.; Chen, V.; Darling, S. B. Janus Membranes: Creating Asymmetry for Energy Efficiency. *Adv. Mater.* **2018**, *30*, No. 1801495.
(22) Chang, Z.-m.; Wang, Z.; Shao, D.; Yue, J.; Lu, M.-m.; Li, L.; Ge, M.; Yang, D.; Li, M.-q.; Yan, H.; Xu, Q.; Dong, W.-f. Fluorescent-magnetic Janus nanorods for selective capture and rapid identification of foodborne bacteria. *Sens. Actuators, B* **2018**, *260*, 1004−1011.
(23) Shao, D.; Zhang, X.; Liu, W.; Zhang, F.; Zheng, X.; Qiao, P.; Li, J.; Dong, W. F.; Chen, L. Janus Silver-Mesoporous Silica Nanocarriers for SERS Traceable and pH-Sensitive Drug Delivery in Cancer Therapy. *ACS Appl. Mater. Interfaces* **2016**, *8*, 4303−4308.
(24) Li, J.; Yao, H.; Wang, Y.; Luo, G. One-Step Preparation of Pd-SiO2 Composite Microspheres by the Sol−Gel Process in a Microchannel. *Ind. Eng. Chem. Res.* **2014**, *53*, 10660−10666.
(25) Boujakhrout, A.; Sánchez, E.; Díez, P.; Sánchez, A.; Martínez-Ruiz, P.; Parrado, C.; Pingarrón, J. M.; Villalonga, R. Single-Walled Carbon Nanotubes/Au-Mesoporous Silica Janus Nanoparticles as Building Blocks for the Preparation of a Bienzyme Biosensor. *ChemElectroChem.* **2015**, *2*, 1735−1741.
(26) Wang, F.; Cheng, S.; Bao, Z.; Wang, J. Anisotropic overgrowth of metal heterostructures induced by a site-selective silica coating. *Angew. Chem., Int. Ed.* **2013**, *52*, 10344−10348.
(27) Bagheri, E.; Ansari, L.; Sameiyan, E.; Abnous, K.; Taghdisi, S. M.; Ramezani, M.; Alibolandi, M. Sensors design based on hybrid gold-silica nanostructures. *Biosens. Bioelectron.* **2020**, *153*, No. 112054.
(28) Zhao, Y.; Yang, D.; Hu, H.; Chen, L.; Xu, Y.; Qu, L.; Yang, P.; Zhang, Q. A simple approach to the synthesis of eccentric Au@SiO2 Janus nanostructures and their catalytic applications. *Surf. Sci.* **2016**, *648*, 313−318.
(29) Choi, D. H.; Lee, S. K.; Oh, Y. K.; Bae, B. W.; Lee, S. D.; Kim, S.; Shin, Y. B.; Kim, M. G. A dual gold nanoparticle conjugate-based lateral flow assay (LFA) method for the analysis of troponin I. *Biosens. Bioelectron.* **2010**, *25*, 1999−2002.
(30) Chen, T.; Wang, H.; Chen, G.; Wang, Y.; Feng, Y.; Teo, W. S.; Wu, T.; Chen, H. Hotspot-induced transformation of surface-enhanced Raman scattering fingerprints. *ACS Nano* **2010**, *4*, 3087−3094.
(31) Wang, P.; Wang, R.; Zhang, W.; Su, X.; Luo, H. Novel fabrication of immunochromatographic assay based on up conversion phosphors for sensitive detection of clenbuterol. *Biosens. Bioelectron.* **2016**, *77*, 866−870.
(32) Han, Y.; Lu, Z.; Teng, Z.; Liang, J.; Guo, Z.; Wang, D.; Han, M. Y.; Yang, W. Unraveling the Growth Mechanism of Silica Particles in the Stober Method: In Situ Seeded Growth Model. *Langmuir* **2017**, *33*, 5879−5890.
(33) Park, J. H.; Dumani, D. S.; Arsiwala, A.; Emelianov, S.; Kane, R. S. Tunable aggregation of gold-silica janus nanoparticles to enable contrast-enhanced multiwavelength photoacoustic imaging in vivo. *Nanoscale* **2018**, *10*, 15365−15370.
(34) Zhu, W.; Liu, L.; Yue, Z.; Zhang, W.; Yue, X.; Wang, J.; Yu, S.; Wang, L.; Wang, J. Au Promoted Nickel-Iron Layered Double Hydroxide Nanoarrays: A Modular Catalyst Enabling High-Performance Oxygen Evolution. *ACS Appl. Mater. Interfaces* **2017**, *9*, 19807−19814.
(35) Wang, Z.; Wang, Y.; Lu, M.; Li, L.; Zhang, Y.; Zheng, X.; Shao, D.; Li, J.; Dong, W.-f. Janus Au−mesoporous silica nanocarriers for chemo-photothermal treatment of liver cancer cells. *RSC Adv.* **2016**, *6*, 44498−44505.
(36) Dexuan, W.; Guian, L.; Qingyan, H.; Ziqiang, W.; Liping, P.; Zhonayue, Z.; Hairong, Z. Synthesis of Au-SiO2 Composite Nanospheres and Their Catalytic Activity. *J. Nanosci. Nanotechnol.* **2016**, *16*, 3821−3826.
(37) Cao, Z.; Chen, H.; Shang, Y.; Zhang, Y.; Qi, D.; Ziener, U. Easily recyclable and highly active rice roll-like Au/SiO2 nanocatalysts from inverse miniemulsion. *Colloids Surf., A* **2017**, *517*, 52−62.
(38) Zhao, B.; Huang, Q.; Dou, L.; Bu, T.; Chen, K.; Yang, Q.; Yan, L.; Wang, J.; Zhang, D. Prussian blue nanoparticles based lateral flow assay for high sensitive determination of clenbuterol. *Sens. Actuators, B* **2018**, *275*, 223−229.
(39) Xu, S.; Zhang, G.; Fang, B.; Xiong, Q.; Duan, H.; Lai, W. Lateral Flow Immunoassay Based on Polydopamine-Coated Gold Nanoparticles for the Sensitive Detection of Zearalenone in Maize. *ACS Appl. Mater. Interfaces* **2019**, *11*, 31283−31290.
(40) Shi, C.; Zhao, S.; Zhang, K.; Hong, G.; Zhu, Z. Preparation of colloidal gold immunochromatography strip for detection of methamidophos residue. *J. Environ. Sci.* **2008**, *20*, 1392−1397.
(41) Lee, S. H.; Rusakova, I.; Hoffman, D. M.; Jacobson, A. J.; Lee, T. R. Monodisperse SnO2-coated gold nanoparticles are markedly more stable than analogous SiO2-coated gold nanoparticles. *ACS Appl. Mater. Interfaces* **2013**, *5*, 2479−2484.
(42) Xie, Y.; Zhang, L.; Le, T. An immunochromatography test strip for rapid, quantitative and sensitive detection of furazolidone metabolite, 3-amino-2-oxazolidinone, in animal tissues. *Food Agric. Immunol.* **2017**, *28*, 403−413.

NOTE ADDED AFTER ASAP PUBLICATION

This paper was published ASAP on December 29, 2020, with an error in Figure 4D. The corrected version was reposted December 30, 2020.

https://dx.doi.org/10.1021/acs.jafc.0c06016
J. Agric. Food Chem. 2021, 69, 511−519